THE JOURNAL OF PHYSICAL CHEMISTRY A
A JOURNAL OF THE AMERICAN CHEMICAL SOCIETY

pubs.acs.org/JPCA Article

Spectroscopic Signature of the Carbon−Carbon Coupling Reaction between Carbon Monoxide and Nickel Carbide

Published as part of The Journal of Physical Chemistry A virtual special issue "Xueming Yang Festschrift".

Jianpeng Yang,* Shihu Du, Bangmin Ju, Ziheng Zhang, Gang Li, Jinghan Zou, Juntao Cao, Qiangshan Jing, Hua Xie,* and Ling Jiang*

Cite This: *J. Phys. Chem. A* 2023, 127, 10450−10456 Read Online

ACCESS | Metrics & More | Article Recommendations | Supporting Information

ABSTRACT: Spectroscopic characterization of ketenylidene complexes is of essential importance for understanding the structure−reactivity relationships of the catalytic sites. Here, we report a size-specific photoelectron velocity map imaging spectroscopic study of the reactions of carbon monoxide with nickel carbide. Quantum chemical calculations have been conducted to search for the energetically favorable isomers and to recognize the experimental spectra. The target products with the chemical formula of $NiC(CO)_n^-$ (n = 3−5) are characterized to have an intriguing ketenylidene CCO unit. The evolution from $NiC(CO)_3^-$ to $NiC(CO)_4^-$ involves the breaking and formation of the Ni−C bond and the coordination conversion between the terminal and bridging carbonyls. Experimental and theoretical analyses reveal an efficient C−C bond formation process within the reactions of carbon monoxide and laser-vaporized nickel carbide. This work highlights the pivotal roles played by metal carbides in the C−C bond formation and also proposes new ideas for the design and chemical control of a broad class of complexes with unique physical and chemical properties.

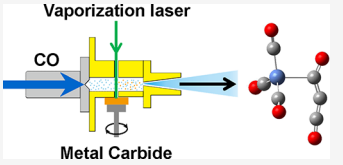

1. INTRODUCTION

The interaction between carbon monoxide (CO) and metals plays a significant role in many fields ranging from fundamental to applied science, such as coordination chemistry, organometallic synthesis, and homogeneous and heterogeneous catalysis.[1,2] Mass-selected gas phase clusters are well-defined models for unraveling the microscopic information on CO chemical adsorption on metal surfaces, the binding of catalyst active sites, and reaction mechanisms. The reaction kinetics, spectral features, and photophysical properties of many unsaturated metal carbonyl substances can be achieved in the cluster studies.[3,4] The coordination modes of CO on metals are mainly divided into three types, such as terminal, bridging, and side-on bond mode. The activation degree of CO is the weakest in terminal coordination, the middle in bridge coordination, and the strongest in side-on coordination.[5]

Studies of metal carbonyls have made remarkable progress in challenging the limitations of the electron-counting rules, with an emphasis on the high-coordination ionic carbonyls of the early transition metals,[6−13] lanthanides,[14] and actinides.[15−19] Neutral alkaline-earth metal octacarbonyls $M(CO)_8$ (M = Ca, Sr, Ba) and group-4 transition metal carbonyls $Ti(CO)_7$ and $TM(CO)_8$ (TM = Zr, Hf) have also been successfully isolated in the solid neon matrix.[20] In addition, undercoordinated transition metal carbonyl clusters have revealed their bonding and vibrational modes, such as $ScCO^{0/-/+}$, Sc_2CO, etc.[21−25] Very recently, confinement-free neutral group-3 transition metal heptacarbonyl $Sc(CO)_7$ and octacarbonyl $TM(CO)_8$ (TM = Y and La) have been identified in the gaseous environment.[26] The investigation of bimetallic carbonyls has characterized a series of intriguing species, such as $MFe(CO)_4^-$ (M = Ti, V, Cr), $TMNi(CO)_n^-$ (TM = Ti, Zr, Hf; n = 3−7), $Ni_2(CO)_n^-$ (n = 4−6).[27−33] It is indicated that the coordination mode of heterotrinuclear $Ti_2Ni(CO)_n^-$ (n = 6−9) carbonyls varies with cluster size.[34] The reaction of CO with metal oxides has received increasing attention, such as $TMO(CO)_n^+$ (TM = Sc, Y, La), $TaNiO(CO)_n^-$ (n = 5−8), $Ni_2TiO_2(CO)_n^-$ (n = 2−4),[35−43] which provide unique insights into the CO activation by metal oxides.

Metal carbides are widely applied in various fields such as catalysis, hydrogen production, and energy storage.[44−46] So far, much less effort has been made to explore the reaction of CO with metal carbide at the molecular level. Herein, we report a photoelectron spectroscopic study of the reaction of CO with nickel carbide in the gas phase. Experimental spectra in combination with theoretical calculations reveal that the $NiC(CO)_n^-$ (n = 3−5) anions contain a ketenylidene CCO unit, indicating that the C−C bond formation proceeds efficiently in the reaction between CO and nickel carbide.

Received: September 14, 2023
Revised: November 21, 2023
Accepted: November 22, 2023
Published: November 30, 2023

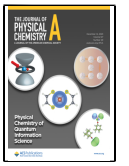

https://doi.org/10.1021/acs.jpca.3c06197
J. Phys. Chem. A 2023, 127, 10450−10456

2. EXPERIMENTAL AND THEORETICAL METHODS

The photoelectron velocity map imaging experiments were implemented with the aid of a self-made apparatus combining a time-of-flight (TOF) mass spectrometer with a double channel and a photoelectron velocity map imaging system. The experimental methods have been detailed previously[47] and are briefly described here. The $NiC(CO)_n^-$ (n = 3−5) products were prepared by laser vaporization of the nickel−carbon (1:1) target in a supersonic expansion of carrier gas (10% CO/He, ∼5 atm) beam produced by a high-pressure pulsed valve. The gas mixture (i.e., carrier gas, CO, anions, cations, and neutrals) is skimmed in a differential chamber. Then, the $NiC(CO)_n^-$ (n = 3−5) anionic clusters were mass-selected by a McLaren Wiley-type TOF spectrometer before being guided into the photodetachment area, where they were intersected by a 355 nm (3.496 eV) laser beam of third-harmonic Nd:YAG laser. The photoelectrons were detected by a microchannel plate (MCP) and a phosphor screen. The photoelectron images were recorded using a high-resolution commercial charged coupling device (CCD) camera. Each raw image, which represents the projection of the photoelectron Newton sphere onto the 2D imaging detector, was obtained by repeating 20,000 laser shots at a repetition rate of 10 Hz. The initial 3D photoelectron distribution was extracted using the Abel Inverse Basis Set Expansion (BASEX) transform method. The calibration of photoelectron spectra was accomplished using the previous result of the Au^- anion, showing an energy resolution of more than 5%.

Theoretical calculations were performed using the Gaussian 16 program.[48] The B3LYP functional was applied using the aug-cc-pVTZ basis set for the C and O atoms[49] and the SDD basis set for the Ni atom[50] (denoted as B3LYP/aug-cc-pVTZ/SDD). Previous studies have indicated that density functional theory calculation with the SDD basis set could yield reliable structural, energetic, and spectral results for nickel carbonyls.[5,27−29] Harmonic frequency analysis ensured that the stable isomers were true local minima on their potential energy surfaces. The vertical detachment energy (VDE) was determined as the energy difference between the anionic structure and the corresponding neutral counterpart in the optimized anionic geometries, while the adiabatic detachment energy (ADE) was computed as the energy difference between the anion and the neutral structure in each optimized structure. The zero-point-energy corrections were considered in the calculations of the relative energies and ADEs.

The photoelectron spectrum for each isomer was simulated based on the generalized Koopman's theorem[51] because this theorem features enhanced simulation accuracy by the introduction of a correction term, which has been rationalized in several studies.[51−55] The spectral simulations in this work were performed by fitting the theoretically obtained VDEs with 0.1 eV width Gaussian functions. Electronic hot bands were not included in the simulated spectra.

3. RESULTS AND ANALYSIS

The 355 nm photoelectron spectra of $NiC(CO)_n^-$ (n = 3−5) are presented in Figure 1, and a representative mass spectrum is shown in Figure S1 in the Supporting Information. The selected photodetachment wavelength allows for the simultaneous observation of the ground states and some excited states for the corresponding neutrals of $NiC(CO)_n^-$ (n = 3−5). The ground-stated VDEs can be readily measured from the electron

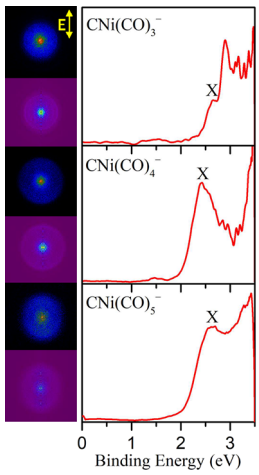

Figure 1. 355 nm photoelectron velocity map imaging of $NiC(CO)_n^-$ (n = 3−5). The left panel shows the raw (upper) and reconstructed images (bottom) after inverse Abel transformation. The double arrow represents the laser polarization direction. The right panel presents the photoelectron spectra obtained from the images.

binding energies (EBEs) of each main band (labeled with X) maximum, which equals 2.70 ± 0.04, 2.43 ± 0.05, and 2.57 ± 0.05 eV for $NiC(CO)_n^-$ (n = 3−5) (Table 1), respectively.

Table 1. Comparison of Experimental VDE/ADE Results to the B3LYP Method of the Five Lowest-Energy Isomers for $NiC(CO)_n^-$ (n = 3−5)

species	isomer	relative energy (eV)	VDE (eV)		ADE (eV)	
			expt.[a]	calc.	expt.[a]	calc.
n = 3	3A	0.00	2.70(4)	2.84	2.50(5)	2.64
	3B	0.38		2.75		2.43
	3C	0.74		2.92		2.61
	3D	1.05		2.85		2.53
	3E	1.32		2.33		1.91
n = 4	4A	0.00	2.43(5)	2.48	2.25(6)	2.33
	4B	0.41		2.80		2.46
	4C	0.52		2.76		2.33
	4D	0.94		2.63		2.23
	4E	1.46		1.93		1.55
n = 5	5A	0.00	2.57(5)	2.60	2.36(6)	2.42
	5B	0.48		3.19		0.94
	5C	0.54		3.00		2.72
	5D	0.80		3.02		2.19
	5E	1.01		2.57		2.03

[a]Numbers in parentheses represent the uncertainty in the last digit.

However, the absence of vibrational structures hinders the direct measurement of ground-state ADEs. Instead, we can estimate these values by determining the intersection of a line along the ascending slope of the main band with the horizontal axis. By this means, the ADE values of $NiC(CO)_n^-$ (n = 3−5) are evaluated as 2.50 ± 0.05, 2.25 ± 0.06, and 2.36 ± 0.06 eV (Table 1), respectively. Thus, their experimental VDE values are more precise than their experimental ADE values. Accordingly, the experimental VDE values were utilized as the main criterion for identifying the isomers.

To unravel the structural information encoded in the observed spectral signature, B3LYP/aug-cc-pVTZ/SDD calculations were performed for both the $NiC(CO)_n^-$ anions and

https://doi.org/10.1021/acs.jpca.3c06197
J. Phys. Chem. A 2023, 127, 10450−10456

the $NiC(CO)_n$ neutrals. The optimized structures of the five lowest-energy isomers for the $NiC(CO)_n^-$ anions are labeled *n*A-*n*E, as shown in Figure 2. The other low-energy isomers of

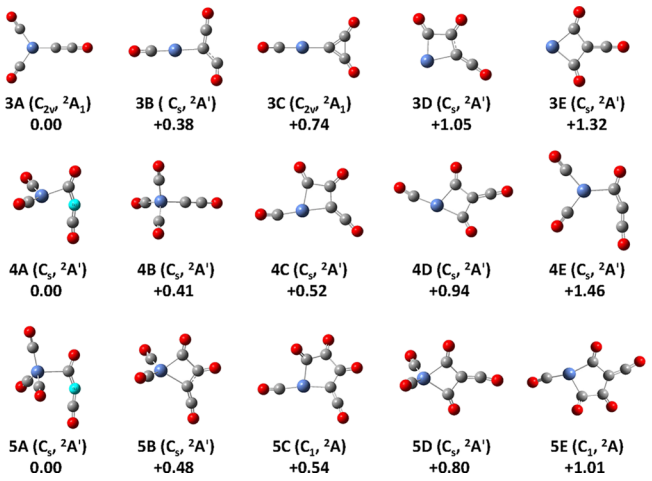

Figure 2. Optimized structures of the five lowest-lying isomers of $NiC(CO)_n^-$ (n = 3−5) calculated at the B3LYP level (Ni, blue; C, gray and baby blue; and O, red). Relative energies are given in eV.

anionic and neutral clusters are illustrated in Figures S2 and S3 in the Supporting Information, respectively. The VDE and ADE values of the *n*A-*n*E isomers are compared with the experimental values in Table 1. Moreover, Figure 3 compares the density of states (DOS) spectra of the *n*A-*n*E isomers simulated based on the theoretically generalized Koopman's theorem with the experimental spectra.

3.1. $NiC(CO)_3^-$. The most stable isomer of $NiC(CO)_3^-$ (labeled 3A) features C_{2v} symmetry with a $^2A_1$ ground state. This isomer includes three terminal carbonyls, in which two directly connect to the Ni atom while the other binds to the C atom. By comparison, the C_s symmetric 3B isomer presents a $^2A'$ state and comprises one terminal carbonyl connecting to the Ni atom and two terminal carbonyls interacting with the C atom. The 3B isomer lies only 0.38 eV higher in energy than 3A. The computed VDE/ADE values of the 3A isomer (2.84/2.64 eV) match well the experimental values (2.70/2.50 eV). A similar agreement between theory and experiment is also obtained for the 3B isomer. The 3C configuration is similar to that of 3B, in which the two carbonyls bound to the C atom to form a C_3 triangle. The 3D isomer consists of a Ni−C−C−C cyclic configuration. The structure of the 3E isomer is similar to that of 3D, but the CCO unit is not directly bound to the Ni atom. The 3C−3E isomers could lie too high in energy to be detected in the experiment. Furthermore, assuming a mixture of the 3A and 3B isomers will best reproduce the experimental spectrum, as shown in Figure S4, implying the coexistence of these two isomers.

3.2. $NiC(CO)_4^-$. For the n = 4 cluster, the lowest-lying 4A isomer contains four carbonyls: a bridging one and three terminal ones (Figure 2), in which two of the terminal carbonyls are linked to the Ni atom, the left terminal carbonyl binds to the C atom, and the original Ni−C bond is broken. To visualize the conversion of structures, the C atom that can react with carbonyls is labeled light blue in Figure 2. The calculated VDE/ADE values for 4A of 2.48/2.33 eV (Table 1) are in accord with the corresponding experimental values (2.43/2.25 eV). The 4B isomer (+0.41 eV) consists of four

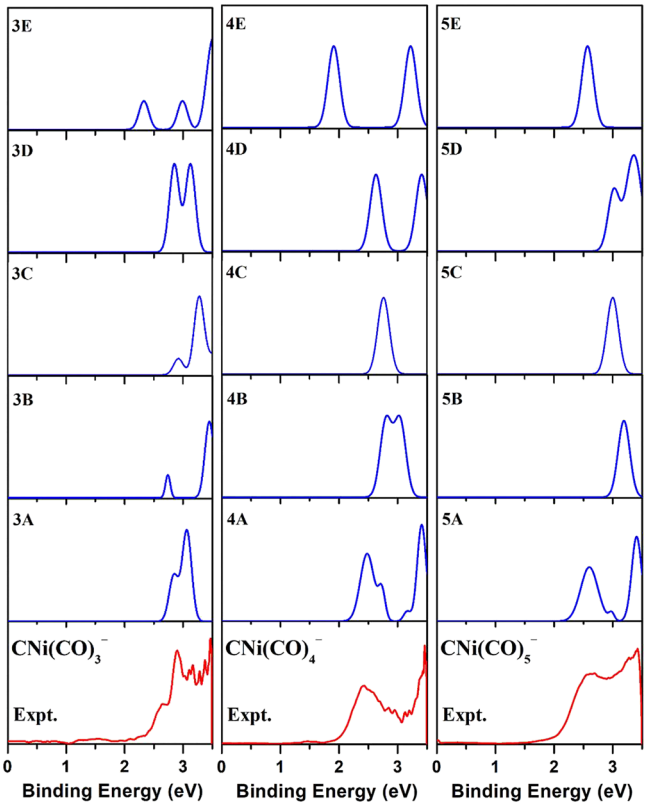

Figure 3. Comparison of experimental 355 nm photoelectron spectra (red line, bottom rows) of $NiC(CO)_n^-$ (n = 3−5) to the simulated spectra of the five lowest-lying isomers (blue line, top five rows).

terminal carbonyls, in which three carbonyls are bound to the Ni atom and the other one is bound to the C atom. The calculated VDE of isomer 4B (2.80 eV) is much higher than the experimental value, indicating that isomer 4B does not contribute to the experimental spectrum. The 4C isomer could be viewed as being built from the 3D isomer by adding a terminal carbonyl connected to the Ni atom. Isomer 4C lies 0.52 eV in energy higher than isomer 4A. The calculated VDE value of isomer 4C (2.76 eV) is also higher than the experimental value (2.43 eV), even though its calculated ADE (2.33 eV) is slightly higher than the experimental value (2.25 eV). Isomer 4D lies 0.94 eV higher in energy than 4A and could be viewed as being built from isomer 3E by adding one terminal carbonyl to the Ni atom. The theoretical VDE value of 4D (2.63 eV) is higher than the experimental result (2.43 eV), while its calculated ADE (2.23 eV) is in agreement with the experimental result (2.25 eV). The structure of isomer 4E is similar to 4A but lies 1.46 eV higher in energy than 4A. The main difference between the structures 4A and 4E lies in the rotation of the $(CO)_2Ni-C$ bond, in which there is a significant difference in the spacing between the Ni atom and the C atom (connected to the two carbonyl groups), as shown in the Figure S5. The calculated VDE/ADE values of 4E (1.93/1.55 eV) are clearly lower compared to the experimental values. Additionally, Figure 3 demonstrates that the simulated 4A spectrum agrees the best with the experimental result in terms of the spectral profile, confirming that 4A is responsible for the $NiC(CO)_4^-$ complex.

3.3. $NiC(CO)_5^-$. For $NiC(CO)_5^-$, the lowest-lying isomer (labeled as 5A) can be regarded as being built from the 4A isomer by introducing another terminally bonded CO group to

https://doi.org/10.1021/acs.jpca.3c06197
J. Phys. Chem. A 2023, 127, 10450−10456

the Ni atom. The calculated VDE/ADE values of 5A are 2.60/2.42 eV (Table 1), respectively, which are very close to the observed values of 2.57/2.36 eV. The 5B (+0.48 eV) and 5C (+0.54 eV) isomers could be regarded as being derived from 4C by terminally bonding CO to the Ni atom and bridging by inserting CO into the Ni−C−C−C ring, respectively. The 5D (+0.80 eV) and 5E (+1.01 eV) isomers could be viewed as being derived from 4D by terminally bonding CO to the Ni atom and bridging inserting CO into the Ni−C−C−C ring, respectively. The computed VDE and ADE values of isomers 5B−5D are discrepant from the experimental results, indicating that the presence of isomers 5B−5D can be ruled out. The 5E isomer lies too high in energy to be experimentally probed. As shown in Figure 3, the agreement between the experimental spectrum and simulated one of the 5A isomers is reasonable to confirm the assignment of 5A to be responsible for the $NiC(CO)_5^-$ complex.

4. DISCUSSION

As shown in Figure S2, the lowest-energy isomer of $NiC(CO)^-$ (labeled 1A) has a terminal carbonyl attached to the C atom. For $NiC(CO)_2^-$, the lowest-lying isomer (labeled as 2A) can be built by terminally bonding another carbonyl to the Ni atom on the basis of 1A. This indicates that the first CO molecule is preferentially bound to the C atom of nickel carbide NiC^-, while the second CO molecule is preferentially bound to the Ni atom of NiC^-.

The agreement of the experimental and theoretical results offers opportunities for investigating the structural evolution of $NiC(CO)_n^-$ (n = 3−5). The coexistence of isomers in $NiC(CO)_3^-$ indicates that the C atom, as a nonmetallic element, can efficiently bond or adsorb CO, demonstrating the unique advantage of the C atom in fixing CO. Due to the coexisting isomers of $NiC(CO)_3^-$, the structural evolution from $NiC(CO)_3^-$ to $NiC(CO)_4^-$ has two patterns of 3A → 4A and 3B → 4A. The 3A → 4A process is characterized by the cleavage of the original C−Ni bond and a bridging carbonyl formation. The 3B → 4A process encompasses adsorption of a terminal carbonyl onto the Ni atom and a transition from a terminal to a bridging carbonyl. These results indicate that the Ni−C bond breaking and formation proceed in the evolution from $NiC(CO)_3^-$ to $NiC(CO)_4^-$. Upon the successive addition of CO, a terminal carbonyl is coordinated to the Ni atom in $NiC(CO)_4^-$, forming $NiC(CO)_5^-$.

The structural evolution of the $NiC(CO)_3$ → $NiC(CO)_5$ neutral counterpart is also distinctive (Figure S3). In the 3A′ → 4A′ evolution, a bridging carbonyl transforms into a terminal carbonyl, while the Ni atom chemically adsorbs another terminal carbonyl. This indicates that the breaking and formation of the Ni−C bond also occurs during the $NiC(CO)_3$ → $NiC(CO)_4$ evolution. 5A′ can be regarded as derived from 4A′ by adding one terminal carbonyl to the Ni atom. Thus, the similarity exists in the structural evolution of the anionic and neutral nickel carbide carbonyls.

To understand the changes of charge distribution with CO addition between these identified structures, natural population analysis (NPA) was carried out, and the results are listed in Table 2. The charge distributions of the Ni atom in the most stable structures of $NiC(CO)_n^-$ (n = 0−5) are −0.426, 0.189, 0.096, −0.437, −0.435, and −0.886, respectively. Additionally, the charge distributions of C and $(CO)_n$ are also concretely displayed. The negative charges can be found to be mainly distributed in the C atoms. From NiC^- to 1A, the negative

Table 2. NPA of the Isomers of $NiC(CO)_n^-$ (n = 0−5) Calculated at the B3LYP/aug-cc-pVTZ/SDD Level of Theory

isomer	NPA charge		
	Ni	C	$(CO)_n$
0A	−0.426	−0.574	
1A	0.189	−0.928	−0.261
2A	0.096	−0.807	−0.289
3A	−0.437	−0.508	−0.055
3B	−0.090	−0.777	−0.133
4A	−0.435	−0.526	−0.039
5A	−0.886	−0.535	0.421

charge is transferred from the Ni atom to the CCO unit. The negative charge is mainly moved from the C atom to the Ni atom from 1A to 2A, which shows a trend similar to the change in charge when 2A to 3A. From 3A to 4A, the charge of each part remains basically unchanged, which is mainly determined by the evolution process of 3A → 4A. From 3B to 4A, the main phenomenon is the transfer of negative charges from $(CO)_n$ and the C atom to the Ni atom. From 4A to 5A, the charge of the C atom remains unchanged, for which the negative charge is primarily transferred from $(CO)_n$ to the Ni atom. As shown in Table S2, the charge distribution change of the Ni atom was mainly related to the terminal carbonyls, indicating that the adsorption of end-on carbonyl in the 4A configuration can greatly promote the electron donation ability of the terminal carbonyls. These results indicate that there are significant differences in the changes in charge distribution during the structural evolution process under different coordination patterns, providing a fundamental basis for studying the fixation of CO.

To clarify the electronic structures of $NiC(CO)_n^-$ (n = 1−5), the molecule orbitals of $NiC(CO)_n^-$ (n = 1−5) from the highest occupied molecular orbitals (HOMOs) down to HOMO-4 are shown in Figure 4. The HOMO orbital of 3A is a π-type bond characteristic with outstanding nickel−carbon to carbonyl donation. Their HOMO-1 and HOMO-4 are delocalized π orbitals mainly involving the carbon−carbon unit. The Ni−C bond in the HOMO-2 and HOMO-3 exhibits an obvious σ orbital. For 3B, the HOMO is delocalized π

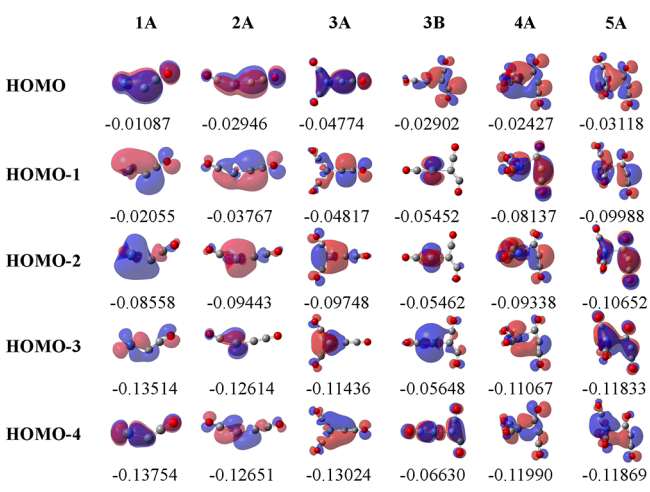

Figure 4. Molecular orbital pictures of $CNi(CO)_n^-$ (n = 1−5), showing the orbitals from HOMO down to HOMO-4. The orbital energies are given in hartree.

https://doi.org/10.1021/acs.jpca.3c06197
J. Phys. Chem. A 2023, 127, 10450−10456

orbitals mainly involving the carbon−carbon unit; the HOMO-1 and HOMO-2 are mainly a 3d orbital of the Ni atom; the HOMO-3 is mainly a 4s orbital of the Ni atom; and the HOMO-4 is a π-type bond trait with salient nickel−carbon to the donated carbonyl. Overall, the weakening of the C−O bond in CO is mainly caused by the effect of π^* back-donation. Similar bonding features have also been observed in the *n*A (n = 1−5) isomers (Figure 4). The bonding analyses reveal that the C−O bonds in $NiC(CO)_n^-$ (n = 1−5) are significantly weakened.

The observation of the CCO unit is quite interesting because the ketenylidene complexes are key intermediates in many catalytic processes.[56] In fact, progress has been made in the synthesis and spectroscopic characterization of a few metal ketenylidene complexes on well-defined surfaces.[57−61] A well-known example is the gold ketenylidene species generated by partial oxidation of acetic acid on a nano-Au/TiO_2 catalyst.[62] Recently, infrared spectroscopy provided evidence of neutral titanium ketenylidene $OTiCCO(CO)_{n-2}$ (n = 4−7) formed from the reactions between CO and titanium atoms.[63] As shown in Table S1, our theoretical calculations show that the stepwise reaction of NiC^- + nCO → $NiC(CO)_n^-$ is highly exothermic, indicating that the formation of CCO from the reactions of CO with nickel carbide is facile in the gas phase. These findings have important implications for understanding the structure−reactivity relationship of metal catalysts toward CO molecules.

5. CONCLUSIONS

The reactions of CO with nickel carbide have been studied by combining photoelectron velocity map imaging and quantum chemical calculations, which reveal the geometric and electronic structures of the $NiC(CO)_n^-$ (n = 3−5) products via thorough energetics comparison and spectral assignments. The results indicate that CO addition to the C center is favored over addition to the Ni center, resulting in the formation of the CCO unit. During the process from $NiC(CO)_3^{-/0}$ to $NiC(CO)_4^{-/0}$, the cleavage and generation of the Ni−C bond and the conversion between terminal and bridging carbonyl ligands are observed. Bonding analysis shows that the C−O bonds in $NiC(CO)_n^-$ (n = 3−5) are significantly weakened. These findings offer new insights into the structural and bonding mechanism of CO with metal carbides, which advance our understanding of CO activation and stimulate further study of a wide range of novel compounds with unique structures and properties.

■ ASSOCIATED CONTENT

Supporting Information

The Supporting Information is available free of charge at https://pubs.acs.org/doi/10.1021/acs.jpca.3c06197.

Mass spectra; optimized structures of low-lying isomers of anionic $NiC(CO)_n^-$ and neutral $CNi(CO)_n$; comparison of experimental 355 nm photoelectron spectrum of $CNi(CO)_3^-$ to the simulated total spectra of 1.3 (3A): 1 (3B) mixture of isomers; spacing of Ni−C in the 4A and 4E structures; reaction energies; natural population analysis of the 4A and 5A isomers; and Cartesian coordinates of selected low-lying isomers of $NiC(CO)_n^-$ (n = 3−5) (PDF)

■ AUTHOR INFORMATION

Corresponding Authors

Jianpeng Yang − *College of Chemistry and Chemical Engineering, Xinyang Normal University, Xinyang 464000, China*; Email: yangjpchem@126.com

Hua Xie − *State Key Laboratory of Molecular Reaction Dynamics, Dalian Institute of Chemical Physics, Chinese Academy of Sciences, Dalian 116023, China*; orcid.org/0000-0003-2091-6457; Email: xiehua@dicp.ac.cn

Ling Jiang − *State Key Laboratory of Molecular Reaction Dynamics, Dalian Institute of Chemical Physics, Chinese Academy of Sciences, Dalian 116023, China*; orcid.org/0000-0002-8485-8893; Email: ljiang@dicp.ac.cn

Authors

Shihu Du − *State Key Laboratory of Molecular Reaction Dynamics, Dalian Institute of Chemical Physics, Chinese Academy of Sciences, Dalian 116023, China*

Bangmin Ju − *State Key Laboratory of Molecular Reaction Dynamics, Dalian Institute of Chemical Physics, Chinese Academy of Sciences, Dalian 116023, China*

Ziheng Zhang − *State Key Laboratory of Molecular Reaction Dynamics, Dalian Institute of Chemical Physics, Chinese Academy of Sciences, Dalian 116023, China*

Gang Li − *State Key Laboratory of Molecular Reaction Dynamics, Dalian Institute of Chemical Physics, Chinese Academy of Sciences, Dalian 116023, China*; orcid.org/0000-0001-5984-111X

Jinghan Zou − *State Key Laboratory of Molecular Reaction Dynamics, Dalian Institute of Chemical Physics, Chinese Academy of Sciences, Dalian 116023, China*

Juntao Cao − *College of Chemistry and Chemical Engineering, Xinyang Normal University, Xinyang 464000, China*; orcid.org/0000-0002-8983-4655

Qiangshan Jing − *College of Chemistry and Chemical Engineering, Xinyang Normal University, Xinyang 464000, China*

Complete contact information is available at: https://pubs.acs.org/10.1021/acs.jpca.3c06197

Notes

The authors declare no competing financial interest.

■ ACKNOWLEDGMENTS

The authors thank the Dalian Coherent Light Source (DCLS) for support and assistance. The work has been well funded from the National Natural Science Foundation of China (grant nos. 22125303, 92061203, 22273101, 22373102, 22288201, and 21327901), the Youth Innovation Promotion Association from the Chinese Academy of Sciences (CAS) (2020187), the Scientific Instrument Developing Project of the CAS (no. GJJSTD20220001), and International Partnership Program of the Chinese Academy of Sciences (121421KYSB20170012).

■ REFERENCES

(1) Tsutsui, M.; Ishii, Y. Organotransition-Metal Chemistry. *Science* **1975**, *188*, 1224−1225.

(2) Tumas, W.; Gitlin, B.; Rosan, A. M.; Yardley, J. T. Olefin Rearrangement Resulting from the Gas-Phase KrF Laser Photolysis of $Cr(CO)_6$. *J. Am. Chem. Soc.* **1982**, *104*, 55−59.

(3) Liu, Z.; Zou, J.; Qin, Z.; Xie, H.; Fan, H.; Tang, Z. Photoelectron Velocity Map Imaging Spectroscopy of Lead Tetracarbonyl-Iron Anion $PbFe(CO)_4^-$. *J. Phys. Chem. A* **2016**, *120*, 3533−3538.

(4) Xie, H.; Zou, J.; Yuan, Q.; Fan, H.; Tang, Z.; Jiang, L. Photoelectron Velocity-Map Imaging and Theoretical Studies of Heteronuclear Metal Carbonyls $MNi(CO)_3^-$ (M = Mg, Ca, Al). *J. Chem. Phys.* **2016**, *144*, 124303.
(5) Zhang, J.; Li, G.; Yuan, Q.; Zou, J.; Yang, D.; Zheng, H.; Wang, C.; Yang, J.; Jing, Q.; Liu, Y.; et al. Photoelectron Velocity Map Imaging Spectroscopic and Theoretical Study of Heteronuclear $MNi(CO)_7^-$ (M = V, Nb, Ta). *J. Phys. Chem. A* **2020**, *124*, 2264−2269.
(6) Ricks, A. M.; Reed, Z. D.; Duncan, M. A. Seven-Coordinate Homoleptic Metal Carbonyls in the Gas Phase. *J. Am. Chem. Soc.* **2009**, *131*, 9176−9177.
(7) Brathwaite, A. D.; Duncan, M. A. Infrared Photodissociation Spectroscopy of Saturated Group IV (Ti, Zr, Hf) Metal Carbonyl Cations. *J. Phys. Chem. A* **2013**, *117*, 11695−11703.
(8) Ricks, A. M.; Brathwaite, A. D.; Duncan, M. A. Coordination and Spin States in Vanadium Carbonyl Complexes ($V(CO)_n^+$, n = 1−7) Revealed with IR Spectroscopy. *J. Phys. Chem. A* **2013**, *117*, 1001−1010.
(9) Zhou, X.; Cui, J.; Li, Z. H.; Wang, G.; Liu, Z.; Zhou, M. Carbonyl Bonding on Oxophilic Metal Centers: Infrared Photodissociation Spectroscopy of Mononuclear and Dinuclear Titanium Carbonyl Cation Complexes. *J. Phys. Chem. A* **2013**, *117*, 1514−1521.
(10) Brathwaite, A. D.; Maner, J. A.; Duncan, M. A. Testing the Limits of the 18-Electron Rule: the Gas-Phase Carbonyls of Sc^+ and Y^+. *Inorg. Chem.* **2014**, *53*, 1166−1169.
(11) Xie, H.; Wang, J.; Qin, Z.; Shi, L.; Tang, Z.; Xing, X. Octacoordinate Metal Carbonyls of Lanthanum and Cerium: Experimental Observation and Theoretical Calculation. *J. Phys. Chem. A* **2014**, *118*, 9380−9385.
(12) Frenking, G.; Zhou, M.; Jin, J.; Xin, K.; Wang, G.; Jin, X.; Yang, T. Octacarbonyl Anion Complexes of Group Three Transition Metals $[TM(CO)_8]^-$ (TM = Sc, Y, La) and the 18-Electron Rule. *Angew. Chem., Int. Ed.* **2018**, *57*, 6236−6241.
(13) Unkrig, W.; Schmitt, M.; Kratzert, D.; Himmel, D.; Krossing, I. Synthesis and Characterization of Crystalline Niobium and Tantalum Carbonyl Complexes at Room Temperature. *Nat. Chem.* **2020**, *12*, 647−653.
(14) Frenking, G.; Zhao, L.; Zhou, M. Octacarbonyl Anion Complexes of the Late Lanthanides $Ln(CO)_8^-$ (Ln = Tm, Yb, Lu) and the 32-Electron Rule. *Chem. − Eur. J.* **2019**, *25*, 3229−3234.
(15) Ricks, A. M.; Gagliardi, L.; Duncan, M. A. Infrared Spectroscopy of Extreme Coordination: The Carbonyls of U^+ and UO_2^+. *J. Am. Chem. Soc.* **2010**, *132*, 15905−15907.
(16) Frenking, G.; Zhou, M.; Zhao, L.; Pan, S.; Chi, C.; Jin, J.; Meng, L.; Luo, M. Octacarbonyl Ion Complexes of Actinides $[An(CO)_8]^{\pm}$ (An = Th, U) and the Role of f Orbitals in Metal-Ligand Bonding. *Chem. − Eur. J.* **2019**, *25*, 11772−11784.
(17) Zhou, M.; Andrews, L.; Charles, W.; Bauschlicher, J. Spectroscopic and Theoretical Investigations of Vibrational Frequencies in Binary Unsaturated Transition-Metal Carbonyl Cations, Neutrals, and Anions. *Chem. Rev.* **2001**, *101*, 1931−1961.
(18) Fielicke, A.; Gruene, P.; Meijer, G.; Rayner, D. M. The Adsorption of CO on Transition Metal Clusters: A Case Study of Cluster Surface Chemistry. *Surf. Sci.* **2009**, *603*, 1427−1433.
(19) Ricks, A. M.; Reed, Z. E.; Duncan, M. A. Infrared Spectroscopy of Mass-Selected Metal Carbonyl Cations. *J. Mol. Spectrosc.* **2011**, *266*, 63−74.
(20) Deng, G.; Lei, S.; Pan, S.; Jin, J.; Wang, G.; Zhao, L.; Zhou, M.; Frenking, G. Filling a Gap: The Coordinatively Saturated Group 4 Carbonyl Complexes $TM(CO)_8$ (TM = Zr, Hf) and $Ti(CO)_7$. *Chem. − Eur. J.* **2020**, *26*, 10487−10500.
(21) Zhou, M.; Andrews, L. Matrix Infrared Spectra and Density Functional Calculations of ScCO, $ScCO^-$, and $ScCO^+$. *J. Phys. Chem. A* **1999**, *103*, 2964−2971.
(22) Pilme, J.; Silvi, B.; Alikhani, M. E. Structure and Stability of M−CO, M = First-Transition-Row Metal: An Application of Density Functional Theory and Topological Approaches. *J. Phys. Chem. A* **2003**, *107*, 4506−4514.
(23) Jiang, L.; Xu, Q. Theoretical Study of the Interaction of Carbon Monoxide with 3d Metal Dimers. *J. Chem. Phys.* **2008**, *128*, 124317.
(24) Liang, B.; Zhou, M.; Andrews, L. Reactions of Laser-Ablated Ni, Pd, and Pt Atoms with Carbon Monoxide: Matrix Infrared Spectra and Density Functional Calculations on $M(CO)_n$ (n = 1−4), $M(CO)_n^-$ (n = 1−3), and $M(CO)_n^+$ (n = 1−2), (M = Ni, Pd, Pt). *J. Phys. Chem. A* **2000**, *104*, 3905−3914.
(25) Zhou, M.; Andrews, L.; Bauschlicher, C. W. Spectroscopic and Theoretical Investigations of Vibrational Frequencies in Binary Unsaturated Transition-Metal Carbonyl Cations, Neutrals, and Anions. *Chem. Rev.* **2001**, *101*, 1931−1962.
(26) Wang, C.; Tian, C.-Y.; Zhao, Y.; Jiang, S.; Wang, T.; Zheng, H.; Yan, W.; Li, G.; Xie, H.; Li, J.; et al. Observation of Confinement-Free Neutral Group Three Transition Metal Carbonyls $Sc(CO)_7$ and $TM(CO)_8$ (TM = Y, La). *Angew. Chem., Int. Ed.* **2023**, *62*, No. e202305490.
(27) Xie, H.; Zou, J.; Yuan, Q.; Zhang, J.; Fan, H.; Jiang, L. Photoelectron Velocity Map Imaging Spectroscopy of Heteronuclear Metal−Nickel Carbonyls $MNi(CO)_n^-$ (M = Sc, Y; n = 2−6). *Top. Catal.* **2018**, *61*, 71−80.
(28) Zou, J.; Xie, H.; Yuan, Q.; Zhang, J.; Dai, D.; Fan, H.; Tang, Z.; Jiang, L. Probing the Bonding of CO to Heteronuclear Group 4 Metal-Nickel Clusters by Photoelectron Spectroscopy. *Phys. Chem. Chem. Phys.* **2017**, *19*, 9790−9797.
(29) Yuan, Q.; Zhang, J.; Zou, J.; Fan, H.; Jiang, L.; Xie, H. Photoelectron Velocity Map Imaging Spectroscopic and Theoretical Study of Heteronuclear Vanadium-Nickel Carbonyl Anions $VNi(CO)_n^-$ (n = 2−6). *J. Chem. Phys.* **2018**, *149*, 144305.
(30) Liu, Z.; Bai, Y.; Li, Y.; He, J.; Lin, Q.; Xie, H.; Tang, Z. Unsaturated Binuclear Homoleptic Nickel Carbonyl Anions $Ni_2(CO)_n^-$ (n = 4−6) Featuring Double Three-Center Two-Electron Ni-C-Ni Bonds. *Phys. Chem. Chem. Phys.* **2020**, *22*, 23773−23784.
(31) Wang, G.; Zhao, J.; Hu, H. S.; Li, J.; Zhou, M. Formation and Characterization of $BeFe(CO)_4^-$ Anion with Beryllium-Iron Bonding. *Angew. Chem., Int. Ed.* **2021**, *60*, 9334−9338.
(32) Jin, X.; Bai, Y.; Zhou, Y.; Wang, G.; Zhao, L.; Zhou, M.; Frenking, G. Highly Coordinated Heteronuclear Calcium-Iron Carbonyl Cation Complexes $[CaFe(CO)_n]^+$ (n = 5−12) with d-d Bonding. *Angew. Chem., Int. Ed.* **2021**, *60*, 13865−13870.
(33) Zhang, J.; Liu, Z.; Li, G.; Fan, H.; Jiang, L.; Xie, H. CO Activation by the Heterobinuclear Transition Metal-Iron Clusters: A Photoelectron Spectroscopic and Theoretical Study. *J. Energy Chem.* **2021**, *63*, 344−350.
(34) Yang, J.; Zhang, J.; Du, S.; Li, G.; Zou, J.; Jing, Q.; Xie, H.; Jiang, L. Photoelectron Imaging Spectroscopic Signatures of CO Activation by the Heterotrinuclear Titanium-Nickel Clusters. *Chin. Chem. Lett.* **2023**, *34*, 107702.
(35) Zhang, J.; Li, Y.; Liu, Z.; Li, G.; Fan, H.; Jiang, L.; Xie, H. Ligand-Mediated Reactivity in CO Oxidation of Niobium-Nickel Monoxide Carbonyl Complexes: The Crucial Roles of the Multiple Adsorption of CO Molecules. *J. Phys. Chem. Lett.* **2019**, *10*, 1566−1573.
(36) Zhang, J.; Li, Y.; Bai, Y.; Li, G.; Yang, D.; Zheng, H.; Zou, J.; Kong, X.; Fan, H.; Liu, Z.; et al. CO Oxidation on the Heterodinuclear Tantalum−Nickel Monoxide Carbonyl Complex Anions. *Chin. Chem. Lett.* **2021**, *32*, 854−860.
(37) Du, S.; Han, H.; Yan, Y.; Lv, Y.; Fan, Z.; Liu, X.; Liang, X.; Xie, H.; Zhao, Z.; Shi, R. Structural and Photoelectron Spectroscopic Study on the Heterotrinuclear Nickel-Titanium Dioxide Carbonyl Complexes $Ni_2TiO_2(CO)_n^-$ (n = 2−4). *RSC Adv.* **2023**, *13*, 3164−3172.
(38) Xie, H.; Liu, Z.; Xing, X.; Tang, Z. Infrared Photodissociation Spectroscopy of $MO(CO)_5^+$ (M = Sc, Y, La and Ce) in the Gas Phase. *Chem. Phys. Lett.* **2015**, *628*, 66−70.
(39) Xie, H.; Liu, Z.; Zhao, Z.; Kong, X.; Fan, H.; Tang, Z.; Jiang, L. Observing the Transition from Equatorial to Axial CO Chemisorption: Infrared Photodissociation Spectroscopy of Yttrium Oxide−Carbonyls. *Inorg. Chem.* **2016**, *55*, 5502−5506.

https://doi.org/10.1021/acs.jpca.3c06197
J. Phys. Chem. A 2023, 127, 10450−10456

(40) Chen, Y.; Xin, K.; Jin, J.; Li, W.; Wang, Q.; Wang, X.; Wang, G. Infrared Photodissociation Spectroscopic Investigation of TMO-$(CO)_n^+$ (TM = Sc, Y, La): Testing the 18-Electron Rule. *Phys. Chem. Chem. Phys.* **2019**, *21*, 6743−6749.
(41) Xu, B.; Zhao, Y.-X.; Ding, X.-L.; He, S.-G. Reactions of $Sc_2O_4^-$ and $La_2O_4^-$ Clusters with CO: A Comparative Study. *Int. J. Mass Spectrom.* **2013**, *334*, 1−7.
(42) Sodupe, M.; Branchadell, V.; Rosi, M.; Bauschlicher, C. W. Theoretical Study of M^+−CO2 and OM^+CO Systems for First Transition Row Metal Atoms. *J. Phys. Chem. A* **1997**, *101*, 7854−7859.
(43) Brathwaite, A. D.; Ricks, A. M.; Duncan, M. A. Infrared Photodissociation Spectroscopy of Vanadium Oxide−Carbonyl Cations. *J. Phys. Chem. A* **2013**, *117*, 13435−13442.
(44) Hunt, S. T.; Milina, M.; Alba-Rubio, A. C.; Hendon, C. H.; Dumesic, J. A.; Roman-Leshkov, Y. Self-Assembly of Noble Metal Monolayers on Transition Metal Carbide Nanoparticle Catalysts. *Science* **2016**, *352*, 974−978.
(45) Gao, Q.; Zhang, W.; Shi, Z.; Yang, L.; Tang, Y. Structural Design and Electronic Modulation of Transition-Metal-Carbide Electrocatalysts toward Efficient Hydrogen Evolution. *Adv. Mater.* **2019**, *31*, No. 1802880.
(46) Zhang, X.; Zhang, M.; Deng, Y.; Xu, M.; Artiglia, L.; Wen, W.; Gao, R.; Chen, B.; Yao, S.; Zhang, X.; et al. A Stable Low-Temperature H_2-Production Catalyst by Crowding Pt on α-MoC. *Nature* **2021**, *589*, 396−401.
(47) Qin, Z.; Wu, X.; Tang, Z. Note: A Novel Dual-Channel Time-of-Flight Mass Spectrometer for Photoelectron Imaging Spectroscopy. *Rev. Sci. Instrum.* **2013**, *84*, No. 066108.
(48) Frisch, M. J. T. G.W.; Schlegel, H. B.; Scuseria, G. E.; Robb, M. A.; Cheeseman, J. R.; Scalmani, G.; Barone, V.; Mennucci, B.; Petersson, G. A., *Gaussian 16, Revision, C.01*; Gaussian, Inc.: Wallingford, CT, 2016.
(49) Dunning, T. H. Gaussian Basis Sets for Use in Correlated Molecular Calculations. I. The Atoms Boron through Neon and Hydrogen. *J. Chem. Phys.* **1989**, *90*, 1007−1023.
(50) Oolg, M.; Stoll, H.; Preuss, H. Energy-Adjusted Ab Initio Pseudopotentials for the Rare Earth Elements. *J. Chem. Phys.* **1989**, *90*, 1730−1734.
(51) Tozer, D. J.; Handy, N. C. Improving Virtual Kohn−Sham Orbitals and Eigenvalues: Application to Excitation Energies and Static Polarizabilities. *J. Chem. Phys.* **1998**, *109*, 10180−10189.
(52) Akola, J.; Manninen, M.; Häkkinen, H.; Landman, U.; Li, X.; Wang, L.-S. Photoelectron Spectra of Aluminum Cluster Anions: Temperature Effects and Ab Initio Simulations. *Phys. Rev. B* **1999**, *60*, R11297−R11300.
(53) Chen, W.-J.; Zhai, H.-J.; Huang, X.; Wang, L.-S. On the Electronic Structure of Mono-Rhenium Oxide Clusters: ReO_n^- and ReO_n (n = 3, 4). *Chem. Phys. Lett.* **2011**, *512*, 49−53.
(54) Zhai, H.-J.; Zhang, X.-H.; Chen, W.-J.; Huang, X.; Wang, L.-S. Stoichiometric and Oxygen-Rich $M_2O_n^-$ and M_2O_n (M = Nb, Ta; *n* = 5−7) Clusters: Molecular Models for Oxygen Radicals, Diradicals, and Superoxides. *J. Am. Chem. Soc.* **2011**, *133*, 3085−3094.
(55) Smith, B. M.; Kubczyk, T. M.; Graham, A. E. Metal Triflate Catalysed Acetal Exchange Reactions of Glycerol under Solvent-Free Conditions. *RSC Adv.* **2012**, *2*, 2702−2706.
(56) Sailor, M. J.; Shriver, D. F. Vibrational Spectroscopic Characterization of the CCO Ligand and the Possible Occurrence of CCO on Surfaces. *J. Am. Chem. Soc.* **1987**, *109*, 5039−5041.
(57) Shriver, D. F.; Sailor, M. J. Transformations of Carbon Monoxide and Related Ligands on Metal Ensembles. *Acc. Chem. Res.* **1988**, *21*, 374−379.
(58) Calderazzo, F.; Englert, U.; Guarini, A.; Marchetti, F.; Pampaloni, G.; Segre, A. $Zr_3Cp_2(O_2CNiPr_2)_6(\mu_3\text{-}O)(\mu_2\text{-}CCO)$, the First Crystallographically Established Ketenylidene Complex: A Model for CO Reductive Cleavage on Metal Surfaces. *Angew. Chem., Int. Ed.* **1994**, *33*, 1188−1189.
(59) Zhou, M. F.; Andrews, L.; Li, J.; Bursten, B. E. Reactions of Th Atoms with CO: The First Thorium Carbonyl Complex and an Unprecedented Bent Triplet Insertion Product. *J. Am. Chem. Soc.* **1999**, *121*, 12188−12189.
(60) Sim, W. S.; King, D. A. Surface-Bound Ketenylidene (CCO) from Acetone Decomposition on Ag{lll}-p(4 × 4)-O. *J. Am. Chem. Soc.* **1995**, *117*, 10583−10584.
(61) Zhou, M. F.; Andrews, L. Reactions of Zirconium and Hafnium Atoms with CO: Infrared Spectra and Density Functional Calculations of $M(CO)_x$, OMCCO, and $M(CO)_2^-$ (M = Zr, Hf; x = 1−4). *J. Am. Chem. Soc.* **2000**, *122*, 1531−1539.
(62) Green, I. X.; Tang, W.; Neurock, M.; Yates, J. T., Jr. Localized Partial Oxidation of Acetic Acid at the Dual Perimeter Sites of the Au/TiO_2 Catalyst-Formation of Gold Ketenylidene. *J. Am. Chem. Soc.* **2012**, *134*, 13569−13572.
(63) Wang, C.; Li, Q.; Kong, X.; Zheng, H.; Wang, T.; Zhao, Y.; Li, G.; Xie, H.; Yang, J.; Wu, G.; et al. Observation of Carbon-Carbon Coupling Reaction in Neutral Transition-Metal Carbonyls. *J. Phys. Chem. Lett.* **2021**, *12*, 1012−1017.

https://doi.org/10.1021/acs.jpca.3c06197
J. Phys. Chem. A 2023, 127, 10450−10456